EPJ Web of Conferences **92**, 02103 (2015)
DOI: 10.1051/epjconf/20159202103

Measurement and visualization of supercritical CO_2 in dynamic phase transition

Hiroyuki Ushifusa[1, a], Kazuaki Inaba[1], Konosuke Sugasawa[1], Kosuke Takahashi[1] and Kikuo Kishimoto[1]

[1] Department of Mechanical Science and Engineering, Tokyo Institute of Technology Ookayama, Meguroku, Tokyo152, Japan

Abstract. A new experimental device was developed to observe and measure dynamical generations of supercritical CO_2 in a chamber. Temperature and pressure were measured locally by thin thermocouple and pressure transducer. The Rayleigh scattering in the chamber was visualized by a high-speed video camera. Heating of the liquid CO_2 was conducted by a ceramic heater from the upper or the lower side of the chamber. In the case of heating from the upper side, temperature profile was stable and generates $scCO_2$ slowly within a few seconds. On the other hand, in the case of heating from the lower side, $scCO_2$ was created faster within a second but natural convection and turbulence were observed. Numerical simulations of the $scCO_2$ creation in a chamber were also performed using the COMSOL Multiphysics with a program package for themophysical properties of CO_2 called the PROPATH. It showed that $scCO_2$ creation in the heating from the upper side was stable due to the gas-like properties of the $scCO_2$ near the heater. In the case of heating from the lower side, density distribution depended on temperature distribution firstly but after natural convection grows, flow in the chamber became disturbed and the density distribution depended not only on temperature distribution but also on the density fluctuation caused by the convection vortexes. Same tendency was observed in experimental results.

1 Introduction

Supercritical fluids have been widely used due to its properties such as gas-like high diffusivity and liquid-like high resolvability. In particular, supercritical CO_2 ($scCO_2$) is used in many fields in terms of its environmental friendly and non-toxic characteristics. Furthermore, product recovery process in the chemical reaction can be accomplished by simple pressure reduction and the recovered CO_2 is reusable. The $scCO_2$ has many applications: accelerating chemical reactions [1], sterilizing bacteria [2], and as an alternative environment-friendly solvent to organic solvents for cleaning [3], food processing, and material extraction. In general, a large quantity of supercritical fluid is consumed at the quasi-static condition in a relatively large chemical plant. These technologies have been improved from an energy saving point of view. However, when these technologies are adopted in the case of low-volume production, the facilities are too large and it is energetically inefficient to maintain the high temperature and pressure [4]. In this sense, instantaneous creation of $scCO_2$ is suitable for the low-volume production and fast chemical reaction. In our previous study, instantaneous (micro-second order) creation of $scCO_2$ in bubble was proposed and we found $scCO_2$ creation in this time regime in pressure based measurement [5]. Quasi-static conditions and physical properties of $scCO_2$ have been already well surveyed in use while dynamic transition of $scCO_2$ has not been well investigated. Thus, it is necessary to reveal when the characteristics of $scCO_2$ appears after the pressure and temperature exceeds the supercritical point for the applications of chemical reaction and so on.

In this paper we investigated dynamic behavior of the phase transition of CO_2 from liquid phase to supercritical phase by measuring temperature and pressure simultaneously as well as observing the Rayleigh scatterings. We developed the experimental device which can dynamically generate $scCO_2$ by heating from either the upper side or the lower side of the chamber by ceramic heater to examine $scCO_2$ creation in milli-to-micro second order. We also evaluated physical properties of CO_2 by using the program package PROPATH provided by Kyushu University [6].

2 Setup and methods

2.1 Experimental setup

[a] Corresponding author: ushifusa.h.aa@m.titech.ac.jp (h.ushifusa@gmail.com)

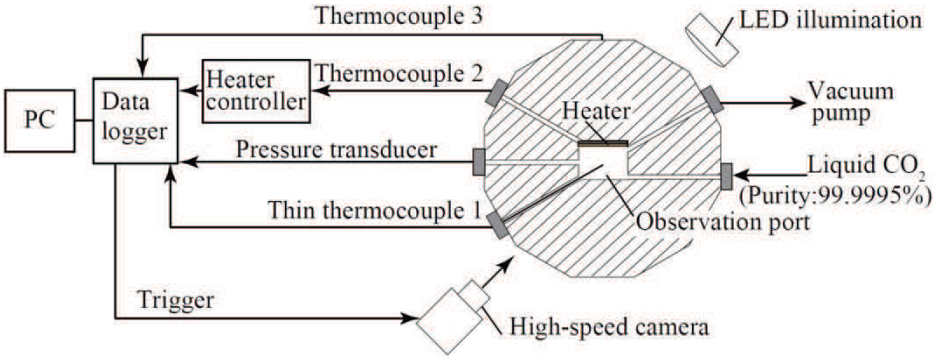

Figure1. Schematic image of experimental setup for $scCO_2$ measurement and observation.

A schematic diagram of the experiment apparatus is shown in figure 1. For creation and observation of $scCO_2$ within a second order, we build a small chamber (20 mm × 14 mm), which is made of SUS304. Liquid CO_2 (purity: 99.9995%) is supplied from CO_2 bombe to the chamber which is vacuumed by vacuum pomp (GVD-050A, Ulvac, Japan) in advance. The pressure and temperature are initially controlled at about 5 MPa and 17 ^{o}C (290.3 K) respectively. Before starting the experiment, liquid CO_2 was heated at nearly 30 ^{o}C. Experiments were started after this operation to heat the fluid (~10 ^{o}C/s) from either the upper side or the lower side of the chamber by a ceramic heater. Temperature surrounding experimental apparatus was controlled around 30 ^{o}C.

The Ceramic heater (MS-1, Sakaguchi, Japan) is controlled by the heater controller (SCR-SHQ-A, Sakaguchi, Japan) with thermo-couple (thermocouple 2). Pressure and temperature in the chamber are measured by the pressure transducer (DPH-L114, Panasonic, Japan) and 25 μm tip thin thermocouple (thermocouple 1) (TSP-K-1000-2, OMEGA, USA). This thermocouple is very sensitive and fragile, thus it is supported by ceramic tube with the tip exposed (figure 2). Wall temperature of the chamber is measured by the thermo-couple 3. These data are collected using the data logger (GL900, Graphtec, Japan) for 10 μs/sample and pressure profile is used as the trigger to control the high-speed camera (VW-9000, KEYENCE Co., Ltd., Japan) to capture the generation of $scCO_2$ visually (Frame rate: 15000 fps, shutter speed: 1/160000 s). The Rayleigh scatterings can be found as transmitted light color change due to the density change when the $scCO_2$ is generated. Every data logged at data logger link to PC and using these data, we estimate thermophysical properties of CO_2 which is calculated by the PROPATH program and the MATLAB software.

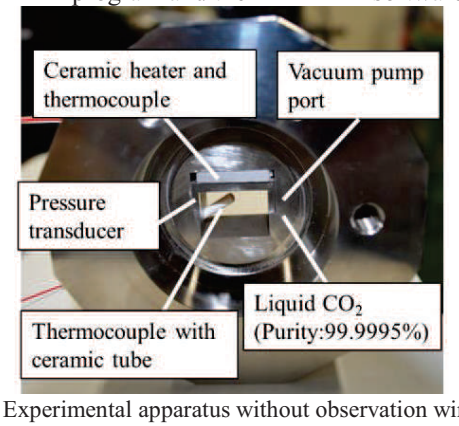

Figure 2. Experimental apparatus without observation window.

In the experimental apparatus, the height of heating position in the chamber can easily modified due to the adjustable jig is in use (figure 3).

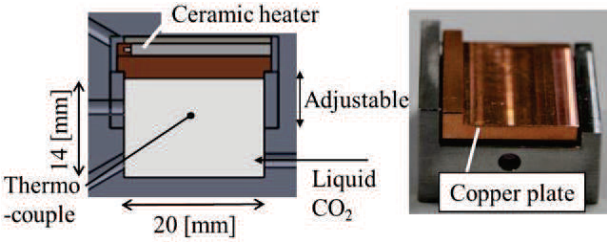

Figure 3. Adjustable heating sections of experimental apparatus.

In this experiment, copper plate was placed upon the SUS304 jig to transfer heat to the liquid CO_2 and height of chamber was 14 mm. Direction of heating is easily changeable, just needs upside down the experimental apparatus. The results obtained by these sensors and high-speed camera are shown in next section.

2.2 Simulation method

Numerical simulation of $scCO_2$ was performed by the COMSOL Multiphysics software to calculate the 2D compressible Navier-Stokes equation with buoyancy force. Thermophysical properties of CO_2 were referred from the PROPATH as functions of temperature and pressure. Equation of state for CO_2 properties of PROPATH is based on International Union of Pure and Applied Chemistry (IUPAC) [7] Schematic image of calculation is given in figure 4. To compare the tendency of fluid motion with experimental results, geometry of calculation area has the same cross section as the experimental apparatus. Density contours are calculated by computational grids (200 × 140) with boundary layers. Liquid CO_2 was heated at constant temperature from the upper side or the lower side. The equation was discretized by the BDF (Backward differential formula) solver where the buoyancy force was taken into account and pressure was at critical pressure of $scCO_2$ (7.38 MPa).

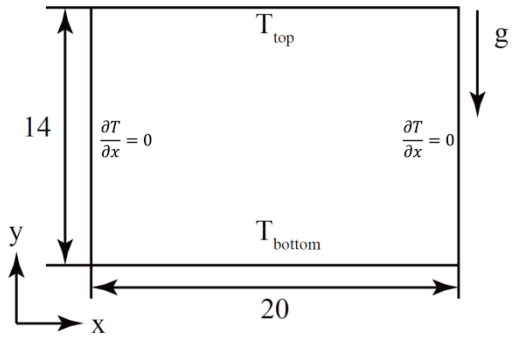

Figure 4. Simulation condition and geometry.

3 Results and discussion

3.1 Experimental results

Liquid CO_2 was heated from top or bottom respectively, which is found in Figure 5, 6. Low pass filter is applied to measured data of temperature and pressure to decrease errors of data.

3.1.1 Heating from the upper side

Figure 5 shows the experimental data and image from high-speed camera of heating from the upper side. The triggered time (1) corresponds to 0 s of the plots in figure 5 when pressure is 0.1 MPa lower than the critical pressure. Green dash lines in plots (a), (b), and (c) are critical
points of each parameter. Image collected by the high-speed camera is also shown in the figure 5(d), and green dash line corresponds to the surface of the heater. The $scCO_2$ area (red dash line) grew very stably and slowly. The creation of $scCO_2$ was observed as black region going down gradually. Owing to the slow and stable creation of $scCO_2$, pressure and temperature profiles are also stable. When pressure and temperature reached their critical points, high-speed camera captured that the tip of thin thermocouple was covered by $scCO_2$ region. At the same time, density calculated by the PROPATH started to decrease as shown in figure 5(c). Large density changes happened within a few seconds, which indicated there is density distribution inside the $scCO_2$ region. This is probably due to the stable temperature distribution in that region.

3.1.2 Heating from the lower side

Figure 6 shows the results heating from the lower side. At the trigger timing, liquid and gas CO_2 are coexisting, and then at the critical temperature, the interface between gas and liquid almost disappeared. After this time, $scCO_2$ region is rapidly expanded to top of the chamber. The motion of fluid was looks like Rayleigh-Bénard convection [8]. Due to its natural convection, temperature indicated large fluctuations caused by the mixture of

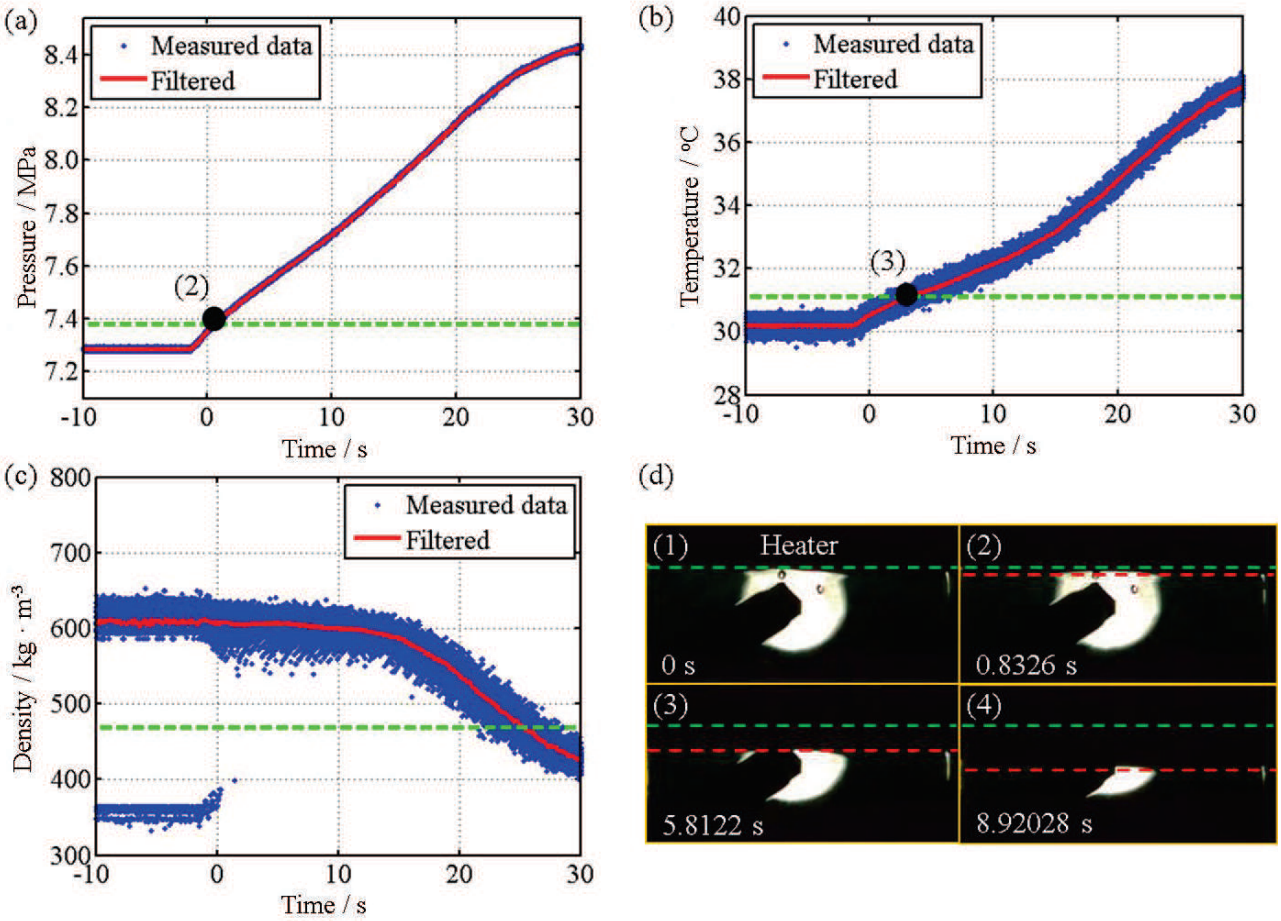

Figure 5. Experimental results of measured temperature and pressure heating from top. Density was calculated using PROPATH. (1) Trigger point, (2) Critical temperature, (3) Critical pressure (Frame rate: 15000 fps, shutter speed: 1/160000 s).

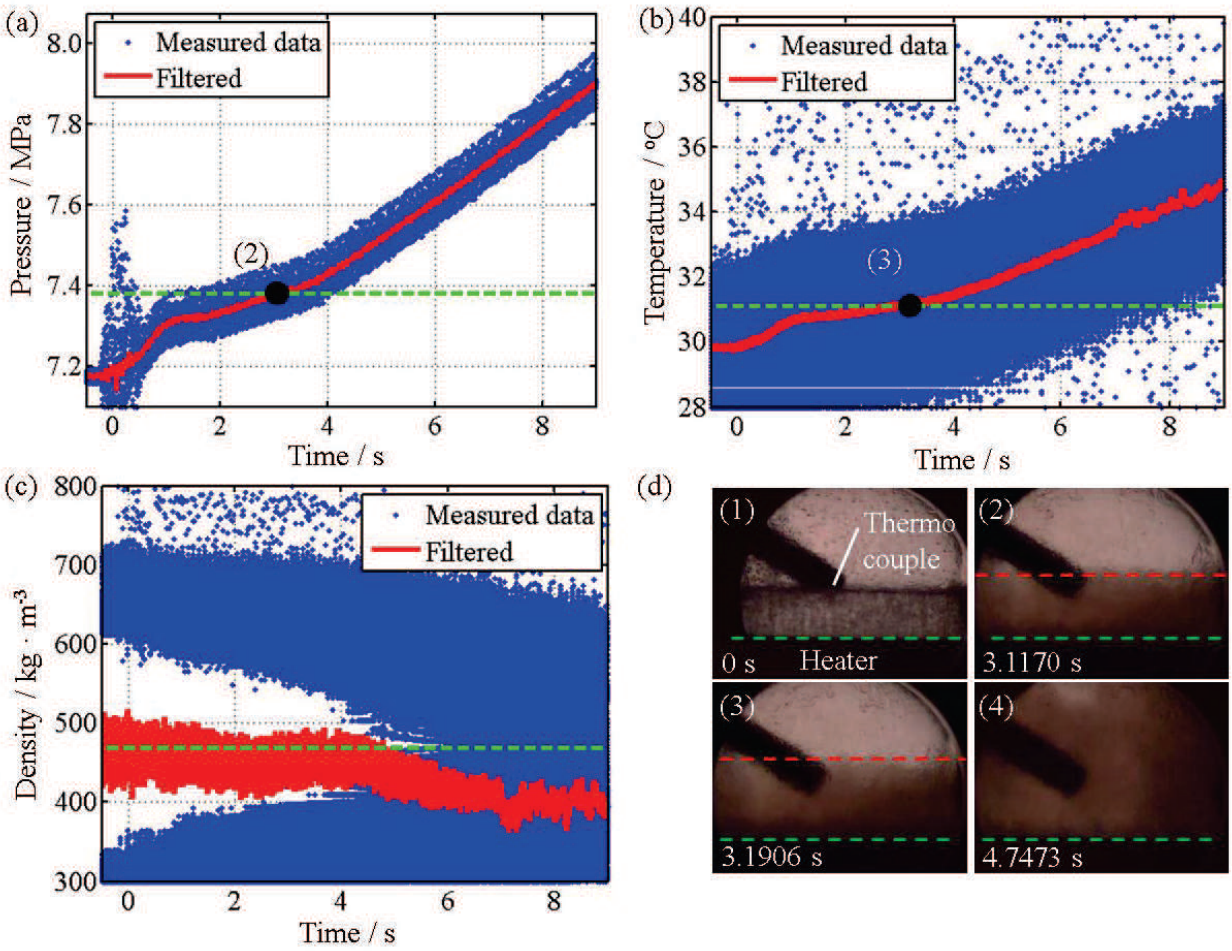

Figure 6. Experimental results of measured temperature and pressure heating from bottom. Density was calculated using PROPATH. (1) Trigger point, (2) Critical temperature, (3) Critical pressure (Frame rate: 10000 fps, shutter speed: 1/30000 s).

liquid and supercritical CO_2, which induced density estimation unstable.

The Rayleigh number was calculated to examine whether this natural convection is density fluctuation domain (Laminar) or turbulent flow domain:

$$Ra = \rho^2 g \beta \Delta T h^3 / \mu \kappa, \quad (1)$$

where ρ is density, g is gravity, β is coefficient of thermal expansion, ΔT is temperature difference between top and bottom walls, h is height observation area, μ is viscosity and κ is thermal conductivity, respectively. These parameters which depend on temperature and pressure are calculated by PROPATH using measured temperature and pressure. According to figure 7, Ra is around 10^{10} at the beginning, and at 2 s, it becomes more than 10^{12}, which means that the flow in the chamber initially indicates critical Rayleigh number and becomes turbulent. After 4 s, the $scCO_2$ region reached the top of the chamber when Ra became the maximum. The turbulence in the chamber creates vortex and makes heat transport larger and 3-times faster than those in the case of heating from the upper side. It is difficult to distinguish density distribution domain scattering (Rayleigh scattering) from turbulent domain scattering, when we observed whole area of the chamber. But before the Bénard cell reach to the top of the chamber (figure 6(d)(4)), there is possibility to measure dynamic density changes using fast pulsed laser focused on small area of $scCO_2$ region.

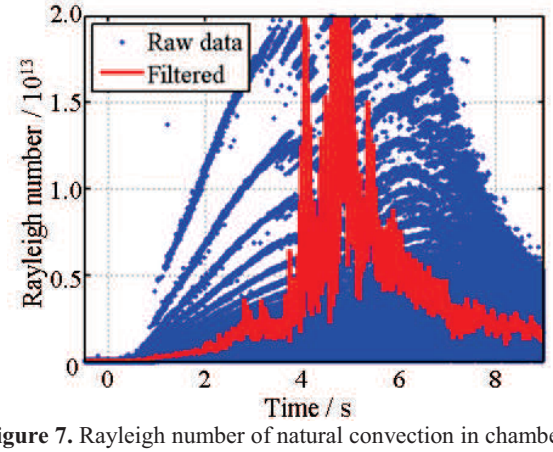

Figure 7. Rayleigh number of natural convection in chamber.

3.2. Simulation results

The experimental results showed that stable heating accomplished by the upper side heating and fast heating by the lower side heating. We discussed both cases of density changes to ensure the possibility to measure fast creation of $scCO_2$. Temperature fluctuation happens when it exceeds the critical point, thus this calculation started

from the heating temperature slightly higher than the critical point. The initial pressure is 7.38 MPa, the critical point of CO_2. When heating from the top of chamber, the top wall temperature T_{top} is 310 K, and the bottom wall temperature T_{bottom} is 300 K. Due to the difficulty of the calculation of supercritical simulation with natural convection, when heating from the bottom, T_{top} is 304 K, and T_{bottom} is 305 K. The stiffness of the calculation was caused by the CO_2 parameters used in the calculation plotted in figure 8.

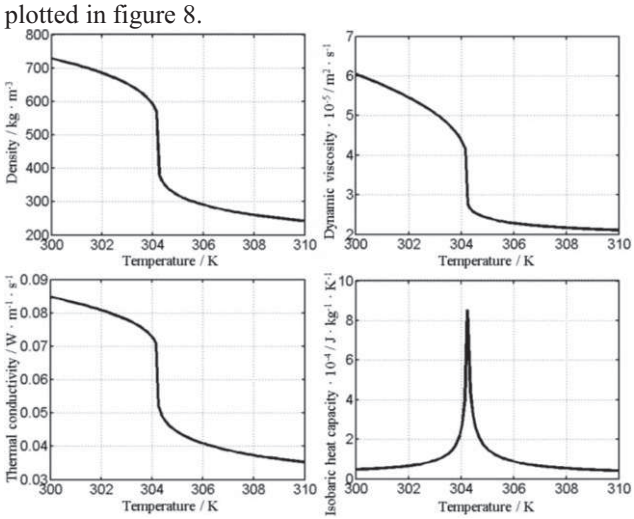

Figure 8. CO_2 parameters calculated by PROPATH.

When liquid CO_2 was heated from the top side, temperature distributions in $scCO_2$ region created density gradient. The region near the heater was gas-like $scCO_2$ and it gradually changed into liquid-like $scCO_2$. It is due to the thermal conductivity decreases with temperature rises, the creation speed of $scCO_2$ decreased as shown in figure 8, 9. The density distribution is stable and it enables us to observe $scCO_2$ creation (figure 10) and the density changes in longer time range.

On the other hand, in the case of heating from the lower side, density shows large fluctuation because the natural convection transports mixture of fluid at various temperatures. Thus density distribution measured at the point (C) in figure 11 was fluctuated (figure 12). When the natural convection flow is well-developed (figure 11(a), (b)), similar profiles are shown in experimental result, in figure 6(d).

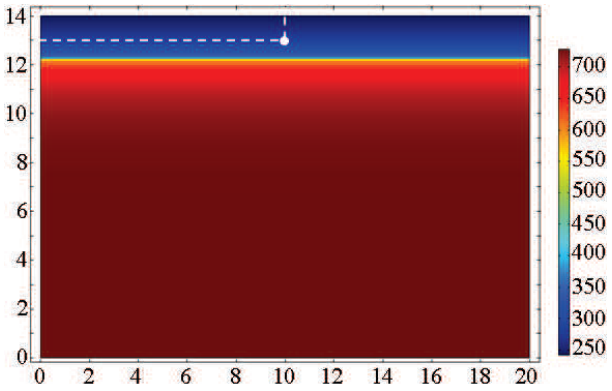

Figure 9. Instantaneous density contours of top heating (100 s from heating and white point is measuring point of density).

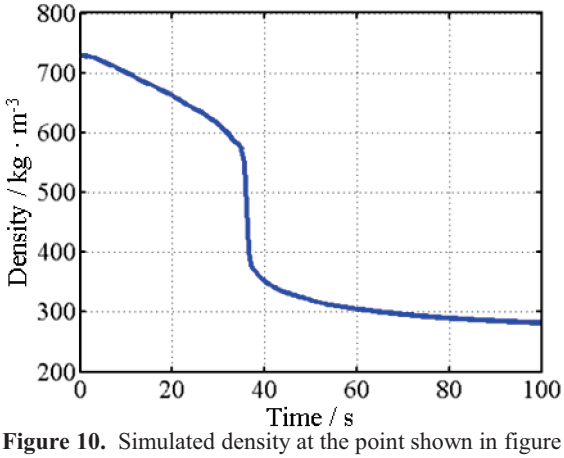

Figure 10. Simulated density at the point shown in figure 9.

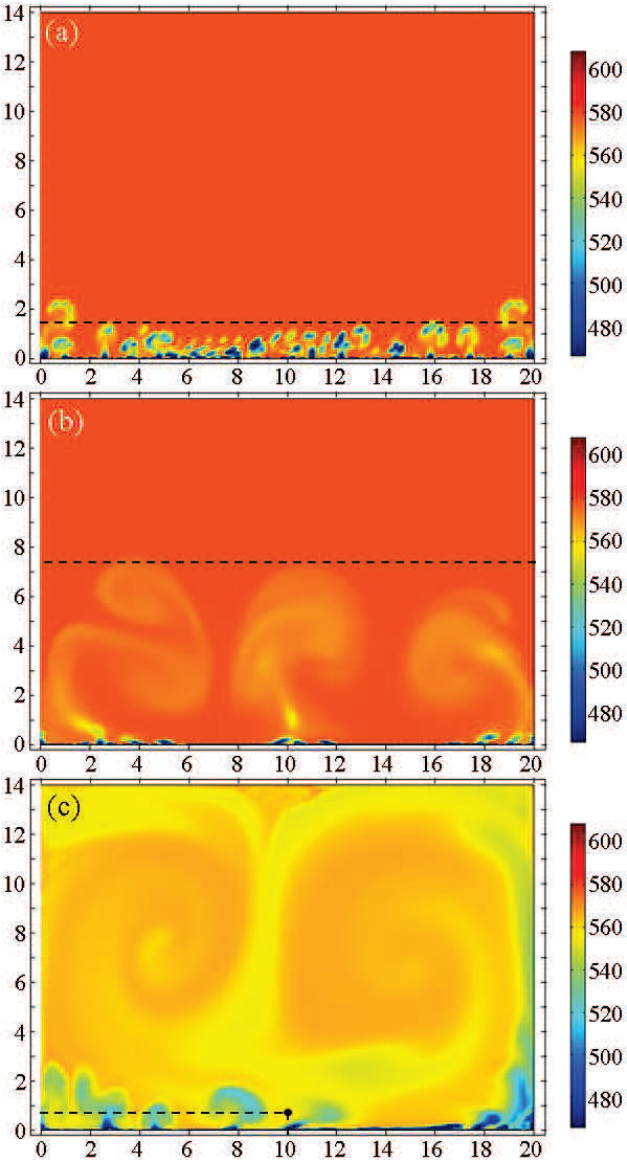

Figure 11. Instantaneous density contours of CO_2 ((a) 0.5 s (b) 1.3 s (c) 10 s after heating started) Black point in (c) is measuring point of density fluctuations.

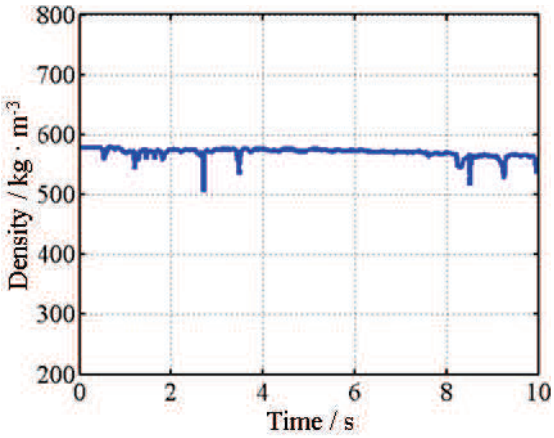

Figure 12. Simulated density at the point shown in figure 11(c).

At figure 11(c), the natural convection was developed due to the temperature gradient in chamber and large density change based on convection vortexes was observed. The numerical simulated density change plotted in figure 12 showed the same tendency with experimental result (see filtered data of figure 6(c)). The numerical results demonstrated the fluid motion clearly which is difficult to observe in the high-speed camera images.

Since the numerical simulations were conducted by assuming the phase transition of the second kind (no superheating and supercooling occur), the density changes of $scCO_2$ in numerical simulations were well followed with temperature and pressure changes. We confirmed that numerical simulations well agreed with experimental results and that the phase transition could be treated as the second kind in a second order. Further experiment is required to confirm that is the density change can be followed with temperature and pressure in shorter time regime, such as micro-to-nano order.

4 Conclusions

Supercritical CO_2 creation using heater was examined by experiments and numerical simulations. The region indicating the Rayleigh scattering was firstly observed near the heater and gradually broadened based on the temperature gradient in the chamber. When the region of the $scCO_2$ (the Rayleigh scattered area) reached at the pressure transducer and the thermocouple, temperature and pressure went beyond the critical condition of $scCO_2$. At the same time, density started to indicate large fluctuations.

Numerical simulations of supercritical fluid were successfully conducted with PROPATH and these results showed the same tendency of density distributions with experimental results. It indicated that the characteristics of $scCO_2$ were confirmed immediately after temperature and pressure satisfied the critical condition within a second order in the phase transition.

References

1. M. Peters, B. Köhler, W. Kuckshinrichs, W. Leitner, P. Markewitz, and T. E. Müller, *ChemSusChem*, **4**, pp. 1216–1240 (2011).
2. White, D. Burns, and T. W. Christensen, *J. Biotechnol.*, **123**, pp. 504–15 (2006).
3. S. Kareth, M. Bilz, J. Mankiewicz, M. Petermann, D. Rebien, and M. Wehrl, *Proceedings of the 10th International Symposium on Supercritical Fluids*, pp. 4–9 (2012).
4. D. Böhm, T. Grau, N. Igl-Schmid, S. Johnsen, E. Kaczowka, A. Klotz, J. Schulmeyr, M. Türk, G. Wiegand, A. Wuzik, and B. Zehnder, *J. Supercrit. Fluids*, **79**, pp. 330–336 (2013).
5. H. Ushifusa, K. Inaba, K. Takahashi, and K. Kishimoto, *J. Supercrit. Fluids*, **94**, pp. 174–181 (2014).
6. PROPATH GROUP, *A Program Package for Thermophysical Properties of Fluids*, **Ver.13.1** (2008).
7. S. Angus, B. Armstrong, K.M. de Reuck, *International thermodynamic table of the fluid state-3 carbon dioxide*, IUPAC 3 (1976).
8. I. Raspo, B. Gilly, S. Amiroudine, P. Bontoux and B. Zappoli, *J. Chim. Phys*, **96**, pp. 1059–1065 (1999).